Available online at www.sciencedirect.com
SCIENCE DIRECT®
Thin Solid Films 451–452 (2004) 624–629
thin solid films
www.elsevier.com/locate/tsf

Nanoporous TiO_2 solar cells sensitised with a fluorene–thiophene copolymer

P. Ravirajan[a,b,*], S.A. Haque[c], D. Poplavskyy[a], J.R. Durrant[c], D.D.C. Bradley[a], J. Nelson[a]

[a]*Department of Physics, Centre for Electronic Materials and Devices, Imperial College London, London SW7 2BW, UK*
[b]*Department of Physics, University of Jaffna, Jaffna, Sri Lanka*
[c]*Department of Chemistry, Centre for Electronic Materials and Devices, Imperial College London, London SW7 2BW, UK*

Abstract

Composites of nanostructured metal oxides with conjugated polymers are promising material combinations for efficient solar energy conversion. However, performance of such combinations is normally limited by the low interfacial area of planar structures and poor charge carrier mobility of the polymer. In this study, we focus on TiO_2 with a high hole-mobility polymer, poly (9,9′-dioctylfluorene-co-bithiophene) (F8T2). Transient optical spectroscopy confirms that efficient photo-induced electron transfer occurs from F8T2 to TiO_2 in both planar TiO_2/F8T2 structures and in high surface area, porous TiO_2/F8T2 structures. Recombination between the positive polaron in the polymer and electron in the TiO_2 is remarkably slow (~ms) in both cases. The influence of layer thickness and surface morphology on cell performance was examined. The best cell was made with reduced layer thickness and increased surface morphology and offered an external quantum efficiency of 11.5% and monochromatic power efficiency of 1 at.% 440 nm. This cell produced an open circuit voltage V_{oc} of 0.80 V and a short circuit current density of approximately 300 $\mu A/cm^2$ under simulated air mass (AM) 1.5 illumination. However, the power conversion efficiency is limited by a poor fill factor, which is attributed to an energy barrier at the polymer/metal interface. We investigate this problem using alternative polymer and top contact metals.

Keywords: Solar cells; Nanostructure; Titanium dioxide; Thiophene; Polymer; Electrodes

1. Introduction

Nanostructured metal oxide films combined with a conjugated polymer overlayer comprise a promising system for low cost photovoltaics. The metal oxide acts as the electron acceptor and transporter in a donor–acceptor heterojunction, and is thus an alternative to fullerene or electron-transporting polymer films. It also offers stability, reasonable electronic conductivity and control of the nanostructured morphology. Simple procedures allow the fabrication of rigid, connected porous metal oxide films, which can be filled with the hole-transporting component to combine electrical connectivity with large interfacial area. Such films are widely studied for use in dye-sensitised solar cells.

Photovoltaic action has been demonstrated previously in 'bi-layer' structures of polymer with TiO_2 [1–3]. In such structures, performance is limited by the low area for charge separation of the planar polymer–TiO_2 interface. Use of a nanostructured metal oxide layer increases the interfacial area and should increase charge separation yield, yet previous attempts were limited by poor polymer penetration into the porous film [4–6], while attempts using dispersed nanocrystals [7,8] were limited because of the poor electron transport between discrete nanocrystals.

In this work, we study structures based on a fluorene–bithiophene copolymer, poly(9,9′-dioctylfluorene-co-bithiophene) (F8T2) and TiO_2 substrates of different morphology. The polymer possesses a high hole-mobility [9] and a liquid crystal phase at 260 °C. We show that polymer penetration into thick porous films can be achieved by melt processing and chemical treatment of the TiO_2 surface. However, better devices are made using thin, spin-coated porous TiO_2 films, in which case

*Corresponding author. Tel.: +44-207-59-47587; fax: +44-207-59-47580.
E-mail address: pr2@imperial.ac.uk (P. Ravirajan).

0040-6090/04/$ - see front matter © 2003 Elsevier B.V. All rights reserved.
doi:10.1016/j.tsf.2003.11.031

penetration is achieved without additional process steps. We report the effect of layer thickness and choice of electronic materials on device performance.

2. Experimental

F8T2 and poly(9,9′-dioctylfluorene-*co*-bis-*N*,*N*′-(4-butylphenyl)-bis-*N*,*N*′-phenyl-1,4-phenylenediamine) (PFB) polymers were dissolved in toluene at concentrations 10–20 mg/ml. Colloidal TiO_2 paste (~15 nm diameter, 50% porosity) was prepared by a sol–gel route as described in Ref. [10].

All samples were prepared on indium tin oxide (ITO) coated glass substrates (~1 cm^2), which were first cleaned by ultrasonic agitation in acetone and isopropanol. The cleaned substrate was then covered with a dense TiO_2 layer that prevents direct contact of polymer with ITO, called the 'Hole blocking layer', using a spray pyrolysis technique [11]. This dense layer prevents direct contact between the polymer and the substrate. For 'thick' multi-layer samples, a 500–1000 nm layer of porous TiO_2 was deposited by doctorblading a colloidal paste in carbowax onto the backing layer. For 'thin' multi-layer samples, a thin porous TiO_2 layer of thickness approximately 100 nm was deposited by spin coating (2000 rpm) a diluted aqueous colloidal paste onto the backing layer. The layers were then sintered at 450 °C for 30 min. The hole-conductor was applied by spin coating a solution of polymer in toluene (10–20 mg/ml) at 1000–2000 rpm, which produced polymer film thicknesses of 50–200 nm. For bi-layer samples, the polymer was spin-coated directly onto the backing layer. The thickness of all the films was measured with a Tencor Alpha-Step 200 profilometer. For electrical characterization, gold or aluminium contacts (~50 nm) were deposited onto the polymer film by evaporation though a shadow mask. Each sample contained six devices of active area 0.042/cm^2. For optical measurements, uncontacted samples on ITO substrates were used.

Photo-induced charge transfer yield and recombination kinetics were measured using nanosecond–millisecond transient optical spectroscopy as described in Ref. [12]. For F8T2/TiO_2 samples, the pump wavelength was 500 nm and the probe wavelength 720 nm. The transient optical spectrum, which peaks at approximately 720 nm, is assigned to the positive polaron in F8T2 after comparison with the absorption spectrum of chemically oxidized polymer. The decay in absorbance as a function of time after the laser pulse is attributed to recombination of F8T2 polarons with electrons in TiO_2.

For electrical measurements the sample was loaded in a home-built sample holder with a quartz window. All measurements were taken under vacuum. The light source was a 100-W xenon lamp, which was driven by a Bentham 505 stabilized power supply. The light from the lamp was dispersed by a CM110, 1/8 m monochromator. Current–voltage (I–V) measurements were taken using a Keithley 237 high voltage source measurement unit with computer control.

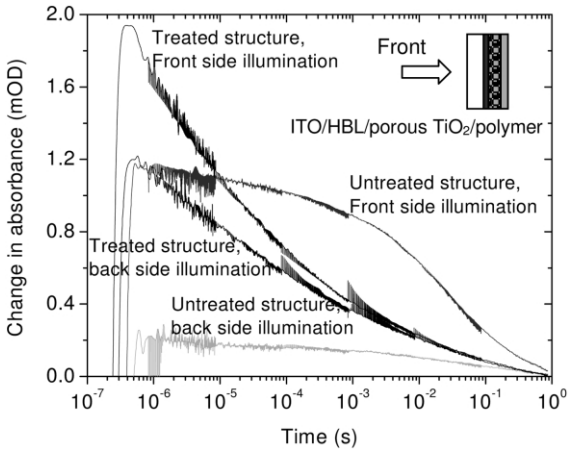

Fig. 1. Transient absorption due to the positive polaron state of the F8T2 polymer at 720 nm following laser pulse excitation at 500 nm, at an excitation density of 50 μJ/pulse/cm^2. The decay is assigned to recombination between electrons in TiO_2 and $F8T2^+$ polarons. Black curves represent transient absorption kinetics for an ITO/dense TiO_2/600 nm porous TiO_2/200 nm F8T2 structure that has been surface treated and annealed. Grey curves are for an untreated structure. The difference between the response for front (TiO_2) and back (polymer) side illumination in the latter case shows that without additional treatments, the spin-coated polymer does not penetrate into the thick (600 nm) porous TiO_2 layer.

External quantum efficiency spectra of the sample were calculated by comparison of the short circuit photocurrent spectrum of the sample with that of a calibrated silicon photodiode (Newport) when measured under the same conditions and at the same position as the sample. Monochromatic I–V curves were taken at the wavelength that gave the highest photocurrent. The I–V characteristic in the dark was measured before and after the illuminated I–V characteristic in order to confirm that the device behaviour had not changed. I–V characteristics were also measured under simulated sunlight using a home-built potentiostat measurement unit with computer control and a halogen lamp calibrated to AM 1.5 equivalent intensity (100 mW/cm^2).

3. Results

3.1. Charge separation and recombination kinetics

Fig. 1 shows the transient absorption signal for two multi-layer samples with 100-nm backing layer, 600-nm porous TiO_2 and 200-nm F8T2 polymer, under laser light intensity of approximately 50 μJ/pulse/cm^2. One sample (black curves) was treated with titanium isopropoxide solution before spin-coating the polymer and was annealed at 300 °C to melt the polymer into the

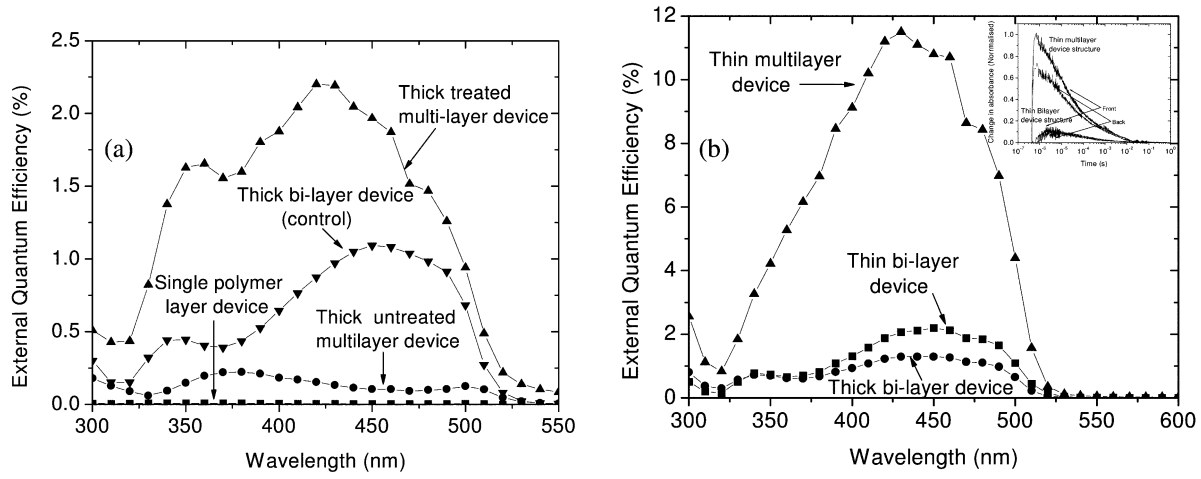

Fig. 2. External quantum efficiency spectra of ITO/TiO_2/F8T2/Au devices with different TiO_2 and polymer layer thickness and surface morphology. (a) Thick bi-layer and multi-layer devices, showing the effect of different process steps. (b) Thin bi-layer and multi-layer devices, showing the strong effect of roughened interface for thin devices. Details of the structures and layer thickness of the corresponding devices are given in Table 1. The insert shows the transient absorption kinetics of thin bi-layer and multi-layer device structures.

pores. The $Ti(iPr)_4$ surface treatment is intended to increase the OH-population on the surface of TiO_2 substrate in order to improve adhesion between TiO_2 surface and the polymer. The second sample (grey curves) was neither surface treated nor annealed. In both cases the transient optical signal is measured for illumination from the back (polymer side) and front sides. Comparison of these signals reveals the extent of polymer penetration into the film. In the case of the untreated sample, the lower signal for back side than front side illumination indicates that less light reaches the charge separating interface for back side illumination. This is attributed to poor polymer penetration into the porous film, leaving a layer of polymer on the back side of the film that attenuates the light reaching the TiO_2/polymer interface. For the treated and annealed sample, the signals for back and front side illumination are similar, indicating effective penetration of polymer into the highly structured TiO_2. The charge separation yield is higher, suggesting better interfacial contact. (We estimate the charge separation yield as close to unity from the polaron extinction coefficient.) However, the faster decay of the signal for the treated sample indicates that recombination is accelerated by the treatments, with the polaron half life reducing from $\sim$10 ms to $\sim$100 μs. This is consistent with more intimate interfacial contact. Nevertheless, the lower value still compares favourably with values reported for polymer–fullerene blends (1–100 μs) [13] and solid dye-sensitised solar cells [12].

In the case of thin multi-layer devices, charge recombination kinetics were very similar to those for the thick treated sample shown here, with similar signals for back and front illumination, and a half life of $\sim$100 μs. However, for thin porous TiO_2 films ($\leqslant$100 nm), similar signal size and kinetics were observed for back and front side illumination without any surface or annealing treatment (Fig. 2b, inset). Treatment did not improve the transient optical signal or the device performance. Therefore, we conclude that effective infiltration of F8T2 polymer into thin porous TiO_2 films is achieved without additional process steps.

3.2. External quantum efficiency

First, bi-layer devices with F8T2 polymer and different metal electrodes are compared. The device with Au electrode generates a photocurrent directed from ITO to metal, with a maximum EQE of approximately 1.3%, while the device with Al electrode generates a negative photocurrent with EQE two orders of magnitude smaller. In the first case, the high work function of Au (nominally 5.1 eV) compared to that of ITO (4.5 eV) establishes an electrostatic driving force attracting holes to the metal and electrons to the ITO. In the case of the Al contact (work function $\sim$4.2 eV) the polarity is reversed and electrons are drawn through the polymer. The very low EQE in this case indicates that TiO_2 is a poor hole-conductor and/or that the polymer is a poor electron-conductor. We conclude that a high work function cathode is needed to collect photocurrent in this system. Note that this is the reverse to most organic solar cell structures, where holes travel to the ITO and a low work function top contact is needed to collect electrons. Studies of Pt contacted devices further support our conclusion [14].

Next we look at the effect of the surface morphology and layer thickness on the EQE. We compare the following devices (summarised in Table 1): bi-layers with two different backing layer thicknesses (50 and

Table 1
Layer thicknesses and peak EQE of devices presented in Fig. 2

Devices	Hole blocking layer (nm)	Porous TiO_2 layer (nm)	Polymer layer (nm)	Peak EQE (%)
Thin bi-layer	50	–	50	2.2
Thick bi-layer	100	–	100	1.3
Thin multi-layer	50	100	75	11.5
Thick multi-layer, untreated	100	600	200	0.2
Thick multi-layer, treated	100	600	200	2.2

100 nm); multi-layer samples similar to those discussed above, with and without treatment steps and an untreated multi-layer sample with thinner backing, porous and polymer layers. All devices were contacted with Au contacts and illuminated through the ITO. The EQE spectra are presented in Fig. 2.

Comparing thin and thick bi-layer devices, the higher EQE of the thin bi-layer device can be attributed to reduced series resistance by the thinner TiO_2 and polymer layer. For both thin and thick layer devices, inserting the porous layer increases the quantum efficiency. This can be attributed to the increased interfacial area for charge separation between TiO_2 and polymer. In the case of the thick multi-layer devices, improved EQE is only achieved after the surface treatment and annealing steps described above. This is consistent with the evidence that such treatments are needed for polymer penetration into the pores of the TiO_2. Without these process steps, the EQE for the thick multi-layer device is worse than that for the control, (probably) due to the lower charge separation yield and the increased series resistance of the additional TiO_2 layer. For thin multi-layer devices, EQE was increased by a factor of 5 to over 11% at peak wavelength. The improvement can be attributed to the increased charge separation yield due to increased interfacial area. The insert of Fig. 2b shows that the magnitude of the transient absorption signal increases by a factor of 5–7 on insertion of the porous TiO_2 layer in the bi-layer structure. The similar kinetics obtained in the multi-layer device for both front and back side illumination confirm that the polymer infiltration is effective in the thin multi-layer device structure.

3.3. Current–voltage characteristics

The current–voltage characteristics of the best device, under simulated sunlight of different intensities and in the dark, are shown in Fig. 3. The device has V_{oc} of 0.8 V and J_{sc} of 0.3 mA/cm^2 under simulated AM 1.5 radiations. However, the current falls off before reaching V_{oc}, leading to a point of inflection or 'kink' in the I–V curve and low fill factor (0.25). Similar shapes of I–V curves have been observed elsewhere for polymer/TiO_2 structures [1,15,16] and molecular film solar cells [17]. We investigated the origin of this effect by varying light intensity, wavelength, polymer and contact metal.

Under increasing light intensity (Fig. 3) the effect becomes more pronounced. This shows that it is not due to an effect of charge trapping in the system, since such effects would become less important, not more, at higher illumination levels. Varying the illumination wavelength while keeping the same photocurrent density allows us

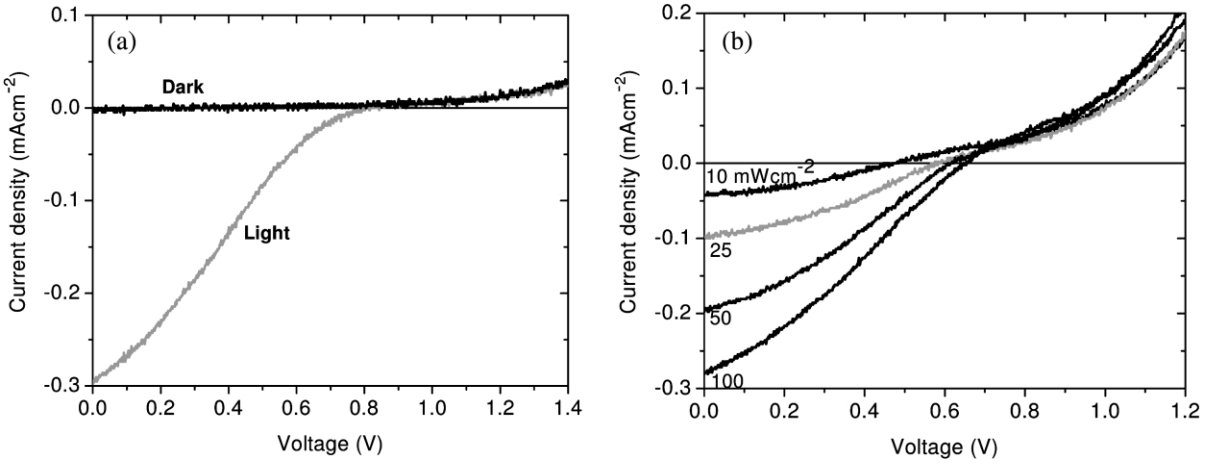

Fig. 3. Current–voltage characteristic of the thin multi-layer device under simulated sunlight (a) comparison of light and dark I–V curves; (b) different light intensities.

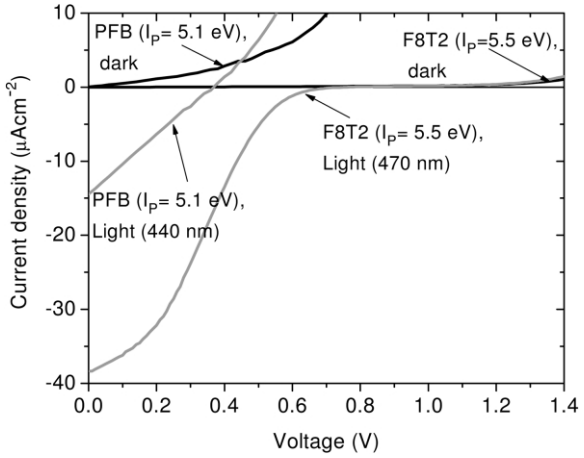

Fig. 4. *I–V* characteristics of ITO/TiO_2/F8T2/Au and ITO/TiO_2/PFB/Au bi-layer devices, under monochromatic illumination and in the dark.

to study the effect of photogeneration profile, to see if the effect is related to a diffusive driving force for photocurrent generation. Varying the wavelength from 470 to 510 nm, which changes the absorption depth from 3×10^5 to 1×10^5/cm, had no observable effect on the shape of the curve (data not shown).

Notice that the dark current for the device is very low in forward bias. This can be explained by the large energy barrier, of approximately 0.5 eV, for hole injection at the metal–polymer interface, which is due to the difference between the HOMO level of F8T2 (ionisation potential 5.5 eV) and the work function of Au (nominally 5.1 eV, but may be less when deposited on polymer). Numerical simulations show that an ohmic injection can be achieved only for barrier heights of approximately 0.3–0.4 eV or less at room temperature [18].

To study whether this energy barrier might also be responsible for the poor fill factor, we varied the energy barrier by using alternative polymers and contact metals. In Fig. 4 light (monochromatic) and dark *I–V* characteristics are presented for two bi-layer devices, one containing 50 nm of F8T2 polymer and the other PFB polymer (ionisation potential 5.1 eV). In the case of the PFB polymer, the dark current is higher, as expected from the much better match of metal work function to the HOMO level of the polymer. The kink has disappeared and the fill factor is better than that for the F8T2 device, although the overall efficiency is lower. The lower V_{oc} for the PFB than the F8T2 device is consistent with easier charge transfer at the Au–polymer contact. (The lower J_{sc} for PFB is mainly due to the lower photon flux at the wavelength used.) Additional studies on ITO/TiO_2/F8T2/Pt devices again showed the increase in dark current and improvement in fill factor, confirming that the effect is indeed due to the polymer–metal interface and not to the polymer–TiO_2 interface [14]. The work function of Pt (5.6 eV) is well matched to the HOMO level of F8T2. An explanation for the origin of the kink in the *I–V* curve is given elsewhere [19].

4. Conclusions

In summary, we have studied charge recombination and photovoltaic device performance in structures consisting of a fluorene–bithiophene copolymer and nanocrystalline TiO_2. Efficient photo-induced charge transfer is observed using a TiO_2 film of high interfacial area, while charge recombination between the hole in the polymer and the electron in the TiO_2 is slow ($\sim$100 μs–10 ms). Polymer penetration into the pores of thin ($<$150 nm) porous TiO_2 films is achieved by spin-coating without any additional processing steps, while additional surface treatment of TiO_2 and melting of the polymer was needed to achieve polymer penetration into pores for thicker TiO_2 films. Photovoltaic devices are made from ITO/TiO_2 backing layer/porous TiO_2/metal contact. Comparison of different (Al and Au) top contacts suggests that high work function top contacts are necessary for efficient photocurrent collection and the energy step between HOMO of the polymer and work function of the top contact must be small for good fill factor. The best performance is achieved with devices with thin ($\sim$100 nm) porous TiO_2 and polymer layers and very thin ($\sim$50 nm) backing layers. Quantum efficiencies of over 11% and monochromatic power conversion efficiencies of approximately 1% are achieved.

Acknowledgments

We are grateful to the Dow Chemical Company for providing the polymers that we have studied and to Alex Green and Emilio Palomares for the preparation of the TiO_2 paste. P.R. acknowledges the Association of Commonwealth Universities for a Commonwealth Scholarship. J.N. acknowledges the EPSRC for the award of an Advanced Research Fellowship.

References

[1] A.C. Arango, L.R. Johnson, V.N. Bliznyuk, Z. Sclesinger, S.A. Carter, H.H. Horhold, Adv. Mater. 12 (2000) 1689.
[2] T.J. Savenije, J.M. Warman, A. Goossens, Chem. Phys. Lett. 287 (1998) 148–153.
[3] Q. Fan, B. McQuillin, D.D.C. Bradley, S. Whitelegg, A.B. Seddon, Chem. Phys. Lett. 347 (2001) 325.
[4] M. Kaneko, K. Takayama, S.S. Pandey, W. Takashima, T. Endo, M. Rikukawa, K. Kaneto, Synth. Met. 121 (2001) 1537–1538.
[5] D. Gebeyehu, C.J. Brabec, F. Padinger, T. Fromherz, S. Spiekermann, N. Vlachopoulos, F. Kienberger, H. Schinder, N.S. Sariciftci, Synth. Met. 121 (2001) 1549–1550.

[6] C.D. Grant, A.M. Schwartzberg, G.P. Smestad, J. Kowalik, L.M. Tolbert, J.Z. Zhang, J. Electroanal. Chem. 522 (2002) 40–48.
[7] A.C. Arango, S.A. Carter, P.J. Brock, Appl. Phys. Lett. 74 (1999) 1698–1700.
[8] J.S. Salafsky, Phys. Rev. B 59 (10) (1999) 885.
[9] H. Sirringhaus, R.J. Wilson, R.H. Friend, M. Inbasekaran, W. Wu, E.P. Woo, M. Grell, D.D.C. Bradley, Appl. Phys. Lett. 77 (2000) 406–408.
[10] R.L. Willis, C. Olson, B. O'Regan, T. Lutz, J. Nelson, J.R. Durrant, J. Phys. Chem. B 106 (2002) 605–7613.
[11] L. Kavan, M. Grätzel, Electrochim. Acta 40 (1995) 643–652.
[12] S.A. Haque, Y. Tachibana, D.R. Klug, J.R. Durrant, J. Phys. Chem. B 102 (1998) 1745–1749.
[13] I. Montanari, A.F. Nogueira, J. Nelson, J.R. Durrant, C. Winder, M.A. Loi, N.S. Sariciftci, C. Brabec, Appl. Phys. Lett. 81 (2002) 3001–3003.
[14] P. Ravirajan, S.A. Haque, D. Poplavskyy, J.R. Durrant, D.D.C. Bradley, J. Nelson, J. Appl. Phys. Rev. B 64 (2001) 125205.
[15] M.Y. Song, J.K. Kim, K.J. Kim, D.Y. Kim, Synth. Met. 137 (2003) 1387–1388.
[16] A.J. Breeze, Z. Schlesinger, S.A. Carter, P.J. Brock, Phys. Rev. B 64 (2001) 125205.
[17] P. Peumans, S.R. Forrest, Appl. Phys. Lett. 79 (2001) 126–128.
[18] P.S. Davids, I.H. Campbell, D.L. Smith, J. Appl. Phys. 82 (1997) 6319.
[19] J. Nelson, J. Kirkpatrick, P. Ravirajan, Phys. Rev. B, accepted.